6508 *Biochemistry* **2010,** *49,* 6508–6518
DOI: 10.1021/bi100670p

BIOCHEMISTRY
including biophysical chemistry & molecular biology
Accelerated Publication

A 1.9 Å Crystal Structure of the HDV Ribozyme Precleavage Suggests both Lewis Acid and General Acid Mechanisms Contribute to Phosphodiester Cleavage[†]

Jui-Hui Chen,[‡,∥] Rieko Yajima,[§,⊥] Durga M. Chadalavada,[§] Elaine Chase,[‡] Philip C. Bevilacqua,*[,§] and Barbara L. Golden*[,‡]

[‡]*Department of Biochemistry, Purdue University, 175 South University Street, West Lafayette, Indiana 47906, and* [§]*Department of Chemistry, Pennsylvania State University, 104 Chemistry Building, University Park, Pennsylvania 16802.* [∥]*Current address: Department of Biochemistry, University of Illinois, 600 S. Mathews Ave., Urbana, IL 61801.* [⊥]*Current address: Research Competitiveness Program, American Association for the Advancement of Science, 1200 New York Ave., NW, Washington, D.C. 20005.*

Received April 30, 2010; Revised Manuscript Received June 16, 2010

ABSTRACT: The hepatitis delta virus (HDV) ribozyme and HDV-like ribozymes are self-cleaving RNAs found throughout all kingdoms of life. These RNAs fold into a double-nested pseudoknot structure and cleave RNA, yielding 2′,3′-cyclic phosphate and 5′-hydroxyl termini. The active site nucleotide C75 has a pK_a shifted >2 pH units toward neutrality and has been implicated as a general acid/base in the cleavage reaction. An active site Mg^{2+} ion that helps activate the 2′-hydroxyl for nucleophilic attack has been characterized biochemically; however, this ion has not been visualized in any previous structures. To create a snapshot of the ribozyme in a state poised for catalysis, we have crystallized and determined the structure of the HDV ribozyme bound to an inhibitor RNA containing a deoxynucleotide at the cleavage site. This structure includes the wild-type C75 nucleotide and Mg^{2+} ions, both of which are required for maximal ribozyme activity. This structure suggests that the position of C75 does not change during the cleavage reaction. A partially hydrated Mg^{2+} ion is also found within the active site where it interacts with a newly resolved G·U reverse wobble. Although the inhibitor exhibits crystallographic disorder, we modeled the ribozyme−substrate complex using the conformation of the inhibitor strand observed in the hammerhead ribozyme. This model suggests that the *pro-*R_P oxygen of the scissile phosphate and the 2′-hydroxyl nucleophile are inner-sphere ligands to the active site Mg^{2+} ion. Thus, the HDV ribozyme may use a combination of metal ion Lewis acid and nucleobase general acid strategies to effect RNA cleavage.

RNA molecules, like their protein counterparts, can fold into stable, compact tertiary structures capable of performing biological catalysis (*1*). Since their discovery nearly 30 years ago, catalytic RNAs, or ribozymes, have been found to function in a wide variety of biological processes, including splicing, translation, gene regulation, and critical RNA processing events, often in the presence of proteins (*2*). The functions of ribozymes are typically Mg^{2+} ion-dependent, and Mg^{2+} can serve both structural and functional roles (*3*).

The ribozymes are often split into two families. Large ribozymes include the group I and group II self-splicing introns and RNase P. These RNAs are generally 200−300 nucleotides in length, have multiple domains, and possess an active site that is large enough to bind RNA duplex substrates and nucleotide or water substrates. They cleave RNA substrates to generate termini with 5′-phosphate and 3′-hydroxyl groups. These ribozymes have been shown to use metal ion catalysis as a key strategy for reaction at phosphodiester centers (*4*−*8*). Metal binding is accomplished by bringing phosphate groups, often from regions distant in the primary structure, into a tight cluster where they create a Mg^{2+} binding pocket. The Mg^{2+} ions participate directly in catalysis by acting as Lewis acids to activate nucleophiles, neutralizing developing charges on leaving groups, and stabilizing the high negative charge of the transition state.

The small nucleolytic ribozymes make up the second major family of RNA catalysts. The hepatitis delta virus (HDV), hammerhead, hairpin, VS, and glmS ribozymes are all naturally occurring members of this family. The small ribozymes are, in general, fewer than 150 nucleotides in length and have evolved to perform single-turnover phosphodiester self-cleavage reactions. All activate a 2′-hydroxyl of an upstream nucleotide for attack at the phosphate group on the following nucleotide (Figure 1A). The products of this strand scission are a 2′,3′-cyclic phosphate and a 5′-hydroxyl group. In contrast to the largely metal-mediated catalysis observed in the large ribozymes, the small ribozymes all appear to use nucleobase catalysis as part of their mechanism (*8*). As a result, these ribozymes can often function in the absence of Mg^{2+} ions if the ionic strength of the surrounding buffer is sufficient to support folding of the RNA (*9*).

The HDV ribozyme (Figure 1B) was initially discovered in the human pathogen HDV, where it is found in closely related genomic and antigenomic forms. It plays a critical role in the viral life cycle, cleaving tandem copies of the RNA genome into single, unit-length pieces (*10*, *11*). Recently, HDV-like ribozymes

[†]This project was supported by National Science Foundation Grant MCB-0527102 to P.C.B., the Purdue University Department of Biochemistry, and the Purdue University Center for Cancer Research.

*To whom correspondence should be addressed. B.L.G.: telephone, (765) 496-6165; fax, (765) 494-7897; e-mail, barbgolden@purdue.edu. P.C.B.: telephone, (814) 863-3812; fax, (814) 865-2927; e-mail, pcb@chem.psu.edu.

 Published on Web 07/20/2010

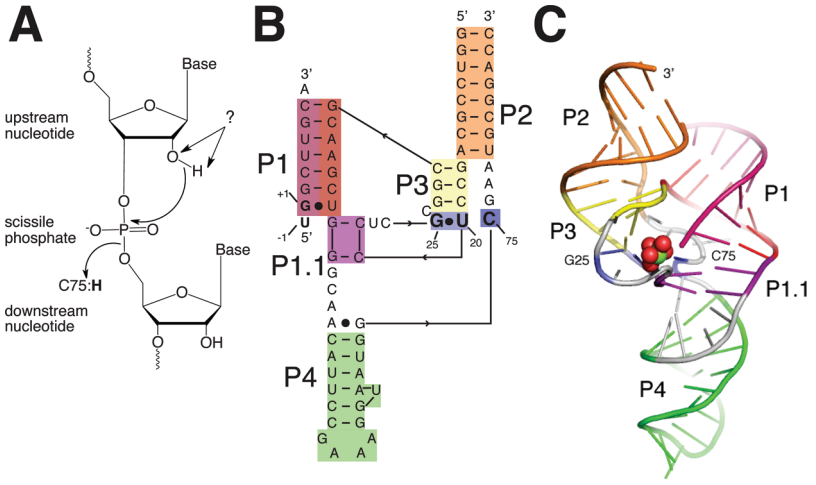

FIGURE 1: HDV ribozyme reaction mechanism and secondary and tertiary structure. (A) In the HDV ribozyme, RNA strand cleavage is catalyzed by activating the 2′-hydroxyl of the upstream nucleotide for attack at the scissile phosphate and by stabilizing the 5′-bridging oxygen leaving group. Biochemical analysis, spectroscopic analysis, and this structural analysis suggest that C75 participates in leaving group stabilization by acting as a general acid. Activation of the 2′-hydroxyl appears to be performed by a Mg^{2+} ion-mediated mechanism; however, the exact nature of the interaction is not fully characterized. (B) Primary and secondary structure of the genomic HDV ribozyme−inhibitor complex used in this study. The sequence is based on a fast-folding, highly reactive HDV ribozyme sequence (*39*) with a GAAA tetraloop introduced into P4 and an extra base pair introduced into P2 to facilitate crystallization. The numbering based on the sequence of the genomic ribozyme is retained. Shown in bold are bases critical to the mechanism, including the nucleotides U(−1) and G1 at the base of P1, a reverse G·U wobble pair at the base of P3, and C75. Paired regions are highlighted with colored boxes. (C) Cartoon rendering of the 1.9 Å crystal structure of the HDV ribozyme. Base-paired double-helical regions are colored as in panel B. C75 is colored dark blue and the G25·U20 reverse wobble light blue. The catalytic Mg^{2+} ion and its hydration shell are shown as spheres. The 3′-end of the inhibitor strand and the 5′-end of the ribozyme strand are close in space, as expected as these two strands are covalently linked in the self-cleaving version of this RNA.

have been discovered throughout all kingdoms of life, including the human genome (*12*, *13*). Therefore, understanding these molecules has implications for human health, mosquito control, and general RNA function in vivo.

The majority of small ribozymes position their cleavage sites by forming base-paired duplexes with the two regions that flank the scissile phosphate. These duplex regions help orient the 2′-hydroxyl of the upstream nucleotide for nucleophilic attack at the scissile phosphate and also facilitate the reverse reaction of ligation by positioning the upstream sequences. In contrast, the HDV ribozyme does not have a guide sequence upstream of the scissile phosphate. As a result, it has proven to be difficult to characterize the upstream portion of the HDV ribozyme, and we currently lack a clear understanding of the interactions necessary to position and activate the 2′-hydroxyl for catalysis. In addition, any nucleotide will serve as the −1 residue in self-cleavage (*14*, *15*), there is little metal specificity to the reaction (*16*, *17*), and a 2′,5′ linkage will be cleaved by the HDV ribozyme (*18*). All of these observations are consistent with limited interactions upstream of the scissile phosphate in the HDV ribozyme.

The HDV ribozymes contain a conserved and catalytically essential cytosine, C75 (numbered C76 in the antigenomic ribozyme), which has a pK_a shifted toward neutrality (*19*−*21*) and whose role as a general acid/base catalyst (*19*, *22*) is key in the mechanism. Nevertheless, despite a number of studies, the role of C75 has not been elucidated from a structural point of view. The first high-resolution picture of this ribozyme came from the structure of a self-cleaving version of the RNA, captured after the reaction, in the product state, and cleaved between U(−1) and G1 (*23*). The structure revealed a complex double, pseudoknotted topology with five pairing elements (Figure 1B), in agreement with solution studies (*24*, *25*). In addition, C75 was poised to accept a hydrogen bond from the 5′-hydroxyl of G1 to its N3 atom. By microscopic reversibility, assuming no significant conformational changes at the active site, C75 would be protonated in the substrate-bound state, suggesting a role as the general acid in phosphodiester bond cleavage (*20*). This role was definitively established by Das and Piccirilli (*26*), who performed key mechanistic studies associating C75 with the leaving group of the ribozyme cleavage reaction.

The role of C75 as a general acid in the cleavage reaction was challenged, however, by the structures of the HDV ribozyme precleavage. To trap the precleaved state, an inactivating C75U mutation was introduced or Mg^{2+} was removed from the reaction mixture (*27*). In contrast to the position of C75 in the product state, these structures revealed an altered active site with U75 in a position to serve as the general base for cleavage, which was supported by molecular dynamics simulations (*28*, *29*). However, interpretation of these structures is clearly complicated by the fact that C75 and Mg^{2+} ions also serve structural roles in the wild-type ribozyme: C75 uses its exocyclic amine to form a hydrogen bond with a phosphate, which cannot be achieved by uracil, and the presence of Mg^{2+} ions alters the conformation of RNA in manners that range from subtle to major. As such, it is likely that a number of catalytically relevant interactions were lost in these structures and were not recovered in molecular dynamics simulations beginning with them.

In an effort to clarify the roles of C75 and Mg^{2+} ion in the mechanism, we report here the structure of a genomic HDV ribozyme trapped in an inhibited, precleavage state. This structure differs from previous studies of the precleaved state, in that the ribozyme contains the native cytosine at position 75 and was determined in the presence of Mg^{2+} ions. The self-cleavage reaction of the ribozyme was inhibited when the 2′-OH nucleophile was changed to a 2′-H. The RNA structure differs significantly from the C75U mutant, is strikingly similar to that of the cleaved form of the ribozyme, and contains a Mg^{2+} ion within the active site. The experimental structure combined with modeling

of the upstream region supports a mechanism in which C75 serves as a general acid and an active site Mg^{2+} ion serves as a Lewis acid in the cleavage mechanism.

EXPERIMENTAL PROCEDURES

Sample Preparation. The RNA was synthesized in two strands. The first strand, formally the ribozyme, spans the 5′-strand of P2 to the 3′-strand of P2, including the 3′-strand of P1 (Figure 1), and was made by T7 transcription. The sequence encoding the ribozyme strand was fused to a T7 promoter and an *Ear*I restriction site, cloned between the *Hin*dIII and *Xba*I restriction sites of pUC-19, and propagated in *Escherichia coli* strain XL-1 Blue. DNA template preparation, RNA synthesis, and RNA purification were performed as previously described (*30*). The ribozyme was exchanged into water or 5 mM potassium cacodylate buffer (pH 6.0), concentrated by ultrafiltration to ~10 mg/mL, and stored at −20 °C.

The second strand, which is formally an inhibitor, spans the 5′-strand of P1 and the cleavage site and was generated by chemical synthesis. To reduce the level of nicking of the inhibitor strand during the crystallization process, three ribonucleotides at the 5′-end were replaced with deoxynucleotides. The sequence of the inhibitor was 5′d(UGG)CUUGCA3′. This RNA was purchased from Dharmacon or Thermo Scientific (Lafayette, CO) and was deprotected and desalted according to the manufacturer's protocols.

Crystallization and Data Collection. To refold the HDV ribozyme−inhibitor complex, equal molar concentrations of ribozyme and inhibitor strands were mixed at a final concentration of 3.5 mg/mL in 5 mM Tris-HCl buffer (pH 7.5). The mixture was heated to 90 °C for 1 min and cooled to room temperature. $MgCl_2$ was added to a final concentration of 10 mM followed by a 10 min incubation at 50 °C. The complex was then allowed to equilibrate at room temperature for 10 min prior to the preparation of crystallization trays.

To obtain crystals of this RNA, 1 μL of the refolded RNA was mixed with an equal volume of reservoir solution containing 50 mM sodium acetate (pH 5.0), 1 mM spermine, and 28−33% 2-methyl-2,4-pentanediol. Low pH was used, as it has been shown that C75 is protonated in these crystals under these conditions (*21*). These drops were equilibrated against 1 mL of the reservoir solution by standard hanging-drop vapor diffusion at 20 °C. Orthorhombic crystals with dimensions of 0.3 mm × 0.05 mm × 0.02 mm were obtained in ~3 weeks. For the collection of cryogenic data, crystals were transferred in a single step to a solution containing 50% 2-methyl-2,4-pentanediol, 50 mM $MgCl_2$, 2 mM spermine, and 50 mM potassium acetate (pH 5.0) for at least 2−3 h. Crystals were then flashed-cooled and stored in liquid nitrogen.

Data were collected at LS-CAT beamline 21-ID-G at the Advanced Photon Source (Argonne National Laboratory, Argonne, IL). Data were processed using HKL2000 (*31*) and indexed in space group $C222_1$.

Phase Determination and Structure Refinement. The initial phases were determined using Phaser, implemented within the CCP4 suite (*32*). The search model was derived from the structure of the cleaved HDV ribozyme from which helix P2 and most of helix P4 had been deleted [Protein Data Bank (PDB) entry 1CX0 (*23*)]. The *Z*-score from the translation function was 8.4, and the LLG was 111. The molecular replacement solution was improved by iterative manual rebuilding and refinement in CNS (*33*, *34*), Phenix (*35*), Pymol (*36*), and O (*37*). Coordinates have been deposited with the Protein Data Bank (entry 3NKB).

RESULTS

The naturally occurring sequence of the HDV ribozyme does not fold into a single, catalytically active population under most conditions. Rather, a significant fraction of this RNA folds into non-native, nonreactive structures whose reactivity is stimulated by chemical denaturants (*25*, *38*). This propensity to misfold complicates analysis of biochemical experiments and can prevent formation of high-quality, catalytically relevant crystals needed for X-ray crystallographic analyses. We therefore initiated crystallization experiments using a fast-folding version of the HDV ribozyme that had been designed to destabilize base pairs within misfolded RNAs without compromising the conformation of the native RNA (*39*). Both self-cleaving and *trans*-cleaving versions of this ribozyme sequence react largely monophasically and rapidly, consistent with homogeneous, native folding (*39*, *40*).

Crystallization Strategies. The earliest published crystallographic studies of the HDV ribozyme focused on a self-cleaving version of the RNA in which a single strand of RNA contains both the active site and the cleavage site. This molecule will efficiently self-cleave, and the first structures of the HDV ribozyme came from the self-cleaved, product form (*23*). To obtain a crystal containing uncleaved RNA with the scissile phosphate and to generate a picture of the ribozyme prior to cleavage, one must prevent the reaction in some fashion. In the previous studies, this was accomplished by a single strand of RNA, using a mutation of the general acid, C75, to uridine (*27*). This sequence variant is completely inactive and has only been shown to function in the presence of imidazole for both antigenomic (*19*) and genomic versions of the HDV ribozyme (*20*).

In this study, we use a *trans*-cleaving ribozyme in which the substrate is provided in an inhibited form as a second RNA strand, held in place by base pairing to the ribozyme. This is a strategy similar to that used to crystallize the hairpin, hammerhead, and glmS ribozymes (*41*−*45*). The substrate is small enough to be efficiently synthesized chemically, which allows us to prevent cleavage by introducing a deoxyribonucleotide at U(−1), the nucleotide upstream of the scissile phosphate. This modification removes the nucleophile and thereby prevents self-cleavage, creating an inhibitor (here termed "inhibitor strand"). In this manner, the atomic structure of the ribozyme active site, including nucleotide C75 and Mg^{2+} ions, remains intact. We have previously demonstrated that this modification leads to crystals that do not alter the pK_a of C75 (*21*) and that have biochemically relevant Mg^{2+} binding (*40*, *46*, *47*). These findings provide confidence that this strategy can be used to capture a picture of the ribozyme bound to a substrate analogue, without disrupting the native interactions that stabilize the active site.

A series of related RNA sequences based on the fast folding variant were generated to introduce mutations into regions of the molecule that could potentially be involved in crystal contacts. The lengths of helices P2 and P4 were varied, and the sequence in L4 was changed. It can be noted that P4 is catalytically dispensable (*15*), and that the lengths of P2 and P4 vary in nature (*13*). This RNA crystallized readily, and a variety of crystal forms were obtained using simple sparse matrix screens. By addition of a base pair to P2, an orthorhombic crystal form was produced, and by variation of cryostabilization conditions,

the diffraction limit was eventually extended to ~1.9 Å resolution (Table 1 and Table S1 of the Supporting Information). This represents significant improvement over the previously determined structures of the HDV ribozyme (*23*, *27*) and is close to the maximal resolution observed for any ribozyme.

The structure was readily determined by molecular replacement, using core base-paired nucleotides from the crystal structure of the self-cleaved HDV ribozyme. The peripheral regions and single-stranded loops were added to the model by iterative rounds of manual model building and energy minimization. The overall geometry of the HDV ribozyme is provided in Figure 1C and is similar to that previously reported (*23*), including the presence of five pairing regions and a topology that results in a double pseudoknot in the *cis*-acting form of the ribozyme.

Table 1: Data Collection and Refinement Statistics

Data Collection	
cell dimensions *a*, *b*, *c* (Å)	64.84, 84.10, 102.02
wavelength (Å)	0.97872
resolution (Å)	50−1.9
R_{sym} (%)[a]	5.5 (42.3)[b]
$I/\sigma(I)$	44.3 (2.2)[b]
no. of reflections	20583
completeness (%)	94.3 (54.6)[b]
redundancy	7.2 (3.4)[b]
Refinement	
resolution (Å)	27−1.9
no. of reflections	20555
no. of reflections in the test set	1999
R_{work}/R_{free} (%)	21.4/24.1 (29.1/31.4)
no. of atoms	
RNA	1538
ion	10
water	169
average *B*-factor	41.2
root-mean-square deviation	
bond lengths (Å)	0.003
bond angles (deg)	1.254
coordinate error (Å)	0.29

[a] R_{sym} is the linear *R*-factor of $\sum|I - \langle I\rangle|/\sum I$, where the *I* is the observed intensity and $\langle I\rangle$ is the average intensity of the multiple observations of symmetry-related reflections. [b] The value for the high-resolution shell is listed in parentheses.

Naturally occurring HDV-like ribozymes are self-cleaving molecules in which the cleaved RNA sequence is covalently linked to the 5′-end of the ribozyme. Although these two strands are separated in the ribozyme−inhibitor complex and are involved in different crystal contacts in the two structures, they remain close in space [~10 Å (Figure 1C)].

One notable feature is found in the new structure: a reverse G·U wobble (*48*) [described as a *trans* W·C/W·C pair by Leontis and Westhof (*49*)] forms between G25 and U20 (Figure 2). In the structure of the product-bound ribozyme [PDB entry 1CX0 (*23*, *50*)], G25 and U20 are coplanar and are oriented such that their Watson−Crick faces could interact; however, in that structure the geometry is not optimal, and they are not within hydrogen bonding distance of each other (the G25 N1−U20 O4 distance is 5.2 Å, and the G25 O6−U20 N3 distance is 4.2 Å). In the C75U mutant structure, U20 interacts with the Hoogsteen face of G25 (*27*). The reverse wobble has been observed in MD studies of the product structure (ref *29*, Veeraghavan, N., P.C.B., and Hammes-Schiffer, S., unpublished data). As in the previous structures, these nucleotides are stacked between the P3 helix and C24, thereby extending the P3 helix. As described below, this reverse wobble plays a critical role in the proposed catalytic mechanism.

At 1.9 Å resolution, Mg^{2+} ions and solvent molecules could readily be incorporated into the model. The electron density in the active site of the ribozyme is rendered in Figure 2.

Although the resolution of the diffraction pattern was quite high, the RNA in the region of the scissile phosphate is disordered. While the electron density for the inhibitor strand at nucleobases from position 1 to 8 is well determined, the position of the backbone for nucleotides 1−3 is somewhat disordered (Figure S1 of the Supporting Information). In addition, continuous density for the upstream nucleotide U(−1) is not visible in electron density maps. There are several potential sources for the disorder observed in the inhibitor strand. First, when RNA from crystals is recovered and analyzed, between 10 and 50% of the inhibitor strand is observed to be nicked (Figure S2 of the Supporting Information). Thus, the disorder could be due to reduced occupancy in this region. Second, disorder may result from the modification of the 2′-hydroxyl nucleophile at position U(−1), or third, it may be inherent to the HDV ribozyme active site (see Discussion).

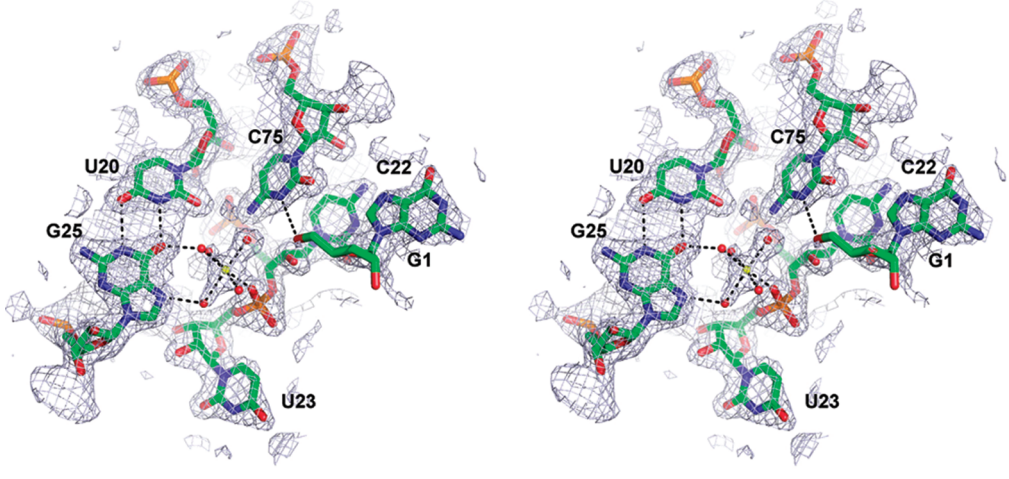

FIGURE 2: Stereoview of the electron density in the region of the active site. The composite simulated annealing omit map is contoured at 1σ within 3 Å of the illustrated atoms.

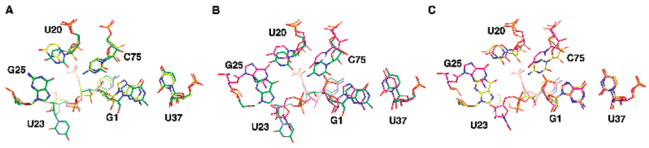

FIGURE 3: Comparison of the active site of the HDV ribozyme in the cleaved, precleaved, and inhibited states. (A) Superposition of the structure of the inhibited ribozyme determined here (green) on the cleaved ribozyme (yellow) (PDB entry 1CX0). Few conformational changes are observed between the cleaved and inhibited states. (B) Superposition of the structure of the inhibited ribozyme determined here (green) on the inactive C75U mutant (PDB entry 1SJ3) (pink) reveals significant conformational changes in the active site. (C) Superposition of the structure of the cleaved HDV ribozyme (PDB entry 1CX0) on the inactive C75U mutant (PDB entry 1SJ3) shows fewer differences than in panel B, but major differences in conformation induced by the C75U mutation are still apparent.

The Position of C75 Suggests That It Serves as the General Acid Catalyst in the Cleavage Reaction. In the crystal structure of the HDV ribozyme in its postcleavage state, C75 is observed to make a hydrogen bond between its N3 atom and the protonated leaving group, the 5′-hydroxyl of G1 (*23*). This conformation suggested that C75 might be protonated in the reactant state, donate its proton to the 5′-O leaving group, and thereby serve as a general acid in the cleavage reaction. This role was supported by experiments in which the phosphodiester linkage between U(−1) and G1 is replaced with a 5′-bridging phosphorothiolate linkage (i.e., 5′-bridging O to 5′-bridging S) (*26*): this modification creates a hyperactive leaving group, and under these conditions, C75 was expendable. This experiment suggests that general acid catalysis is no longer necessary when the leaving group is stabilized and provides strong evidence that C75 serves as a general acid in the cleavage reaction. Mechanistic and spectroscopic analyses provide additional evidence that C75 serves as the general acid in the cleavage reaction (*20*, *21*).

The identification of C75 as a general acid in the solution biochemical studies was confounded somewhat by the crystal structure of the precleaved RNA, trapped in a substrate-bound state by mutation of C75 to uridine (*27*). In this crystal structure, nucleotide 75 is displaced from its binding pocket and can no longer form hydrogen bonds to the 5′-hydroxyl of G1 but instead can be modeled near the 2′-hydroxyl of U(−1). In this manner, nucleotide 75 was implicated as the general base for the cleavage reaction. Molecular dynamics (MD) studies based on this structure appear to support the interpretation that C75 cannot serve as a general acid but rather serves as the general base (*28*, *29*).

It is therefore important to address whether the alternate conformation of nucleotide 75 in the precleaved state was due to the presence of the scissile phosphate or the C75U mutation. We examined the conformation of C75 in our inhibitor-bound structure. In this structure, C75 is in the same conformation as the postcleavage structure, but substantially different from the precleaved structure (Figure 3). The exocyclic amine of C75 hydrogen bonds to the *pro*-R_P phosphoryl oxygen of C22, and its N3 atom is positioned near the 5′-hydroxyl of G1, both interactions being similar to those in the postcleavage structure (*23*). Moreover, the RNA in this region of our structure is very well determined by the diffraction data, with the non-hydrogen atoms in C75 having *B*-factors ranging from just 22 to 30 Å^2. This agreement with our inhibited structure suggests that the position of U75 observed in the precleaved state may be due to the loss of key interactions between the ribozyme core and the exocyclic amine of C75 (which is changed to a carbonyl when C is mutated to U) (*27*).

A Metal Ion Is Found near C75. Solution biochemical studies and Raman crystallographic studies have suggested that there is a Mg^{2+} ion in the active site of the HDV ribozyme (*17*, *40*, *46*, *47*, *51*). Biochemical studies revealed that a 2′,5′ linkage of the scissile phosphate alters the metal dependence of the reaction (*18*), and mutagenesis of the upstream (−1) nucleotide results in an altered divalent metal ion preference (*52*), both suggesting a divalent metal ion is present near position −1. Raman and biochemical studies showed that this Mg^{2+} ion binds anticooperatively with the proton on the N3 atom of C75 (*20*, *21*, *53*), suggesting it is close in space to C75. Moreover, comparison of the pH−rate profiles of the ribozyme in the presence and absence of Mg^{2+} suggests that this Mg^{2+} ion participates in catalysis under biologically relevant conditions (*20*, *51*, *54*). The anticooperative interaction between the active site Mg^{2+} ion and the proton on C75 may be the molecular basis for proposed ground-state destabilization as a driving force for catalysis (*20*).

We observe a partially hydrated Mg^{2+} ion bound within the active site, in the proximity of C75 (Figures 2 and 4). Although electron density for the inhibitor in this region is poor, electron density that can be assigned to the scissile phosphate (Figure S3 of the Supporting Information, overlapping red sphere and green mesh) is visible near the Mg^{2+} ion. A single inner-sphere contact from the ribozyme, the *pro*-S_P oxygen of U23, is also clearly observed between the Mg^{2+} ion and the active site. In addition, this ion interacts through its hydration shell with the N7 and O6 atoms of G25. Thus, the conformation of the G25·U20 reverse wobble is critical to the structure of the active site, and stable base pairing between G25 and U20 may depend on the presence of the Mg^{2+} ion and the scissile phosphate. The remainder of the density was modeled with three waters. At least one of the "water" molecules in the hydration shell exhibits nonspherical electron density. It is likely that this electron density is not water but corresponds to inner-sphere coordination of the scissile phosphate and/or the U(−1) nucleotide in the inhibitor strand. The crystallographic data alone, however, do not allow unambiguous assignment of this electron density to atoms from the inhibitor strand.

If this Mg^{2+} ion represents the catalytic Mg^{2+} ion, then three predictions can be made. First, the conformation of the reverse G·U wobble should be critical to active site structure. Mutation of G25 to an A is predicted to destabilize the Mg^{2+} ion binding site by changing the geometry of the base pair from reverse wobble to reverse Watson−Crick and by reducing the electronegativity in the active site. The Westhof and Been laboratories have shown that this variant is 50−3000-fold less reactive than the parental, wild-type (WT) sequence (*14*, *55*). Moreover, mutation of U20 to an A or a C resulted in at least 10^4-fold less activity (*14*). It is also notable that U20 and G25 are two of only six invariant positions found in all HDV-like ribozymes (*13*).

Second, we expect that this Mg^{2+} ion would be displaced by $Co(NH_3)_6^{3+}$. $Co(NH_3)_6^{3+}$ is a mimic of a hydrated metal ion that can displace both outer- and inner-sphere Mg^{2+} ions (*47*) and strongly inhibits HDV ribozyme activity under biologically relevant Mg^{2+} ion-containing buffer conditions (*51*). Inhibition of the HDV ribozyme by $Co(NH_3)_6^{3+}$ has been shown to be competitive with Mg^{2+} ion (*20*), suggesting a $Co(NH_3)_6^{3+}$ binding site overlaps with a Mg^{2+} ion that is critical for catalysis.

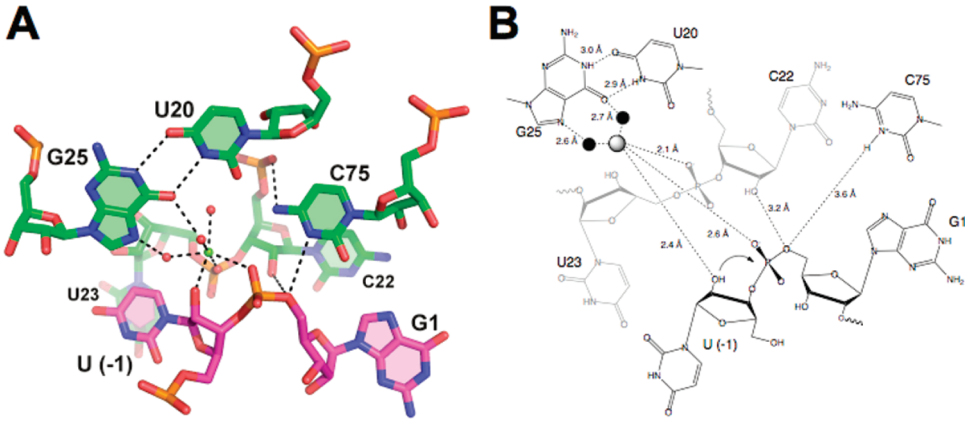

FIGURE 4: Proposed model for the upstream nucleotide and the scissile phosphate. (A) Model for the substrate-bound state of the HDV active site. The model was generated by superposing the cleavage site from the hammerhead ribozyme [pink, PDB entry 2OEU (*43*)] with G1 from the HDV−inhibitor complex (not shown). The active site nucleotides from the crystal structure of the HDV inhibitor complex are colored green. No further adjustments to the conformation were made. This model suggests that the *pro*-R_P oxygen from the scissile phosphate and the 2′-hydroxyl of U(−1) are ligands to the catalytic Mg^{2+} ion (green sphere). (B) Schematic of the contacts shown in panel A. The catalytic Mg^{2+} ion is drawn as a gray sphere, and water molecules are shown as black circles. For the sake of clarity, one water ligand to the catalytic Mg^{2+} ion is not shown. Distances are from the model shown in panel A and differ slightly from those derived from the refined crystal structure (Table 2). The Mg^{2+}−water distance is 2.3 Å for all three water ligands to the catalytic Mg^{2+} ion (Table 2). An arrow indicates in-line attack of the 2′-hydroxyl of U(−1) at the scissile phosphate.

Finally, Raman spectroscopic characterization of $Co(NH_3)_6^{3+}$ binding to the HDV ribozyme shows that it, like Mg^{2+}, binds anticooperatively with the proton on C75, suggesting that the $Co(NH_3)_6^{3+}$ binding site is in the proximity of C75 (*47*). Indeed, the location of this Mg^{2+} ion is similar to that observed crystallographically for $Co(NH_3)_6^{3+}$ (PDB entry 1SJF) (*27*), suggesting that $Co(NH_3)_6^{3+}$ and Mg^{2+} ion must compete for this single ion binding site near the reverse G·U wobble.

Third, the distance from the active site Mg^{2+} ion to the N3 atom of C75 is 5.5 Å. There is strong evidence that these two species interact electrostatically, as mentioned above. This distance is well within the range for through-space electrostatic coupling in RNA (*56*), further supporting the catalytic relevance of this ion. Collectively, the three observations described above indicate that the Mg^{2+} ion observed in the crystal structure has properties similar to that of the catalytic Mg^{2+} ion inferred from solution biochemical studies.

Building a Model for the Upstream Nucleotide. Electron density for nucleotides U(−1) and part of G1 was poor, which precluded building a model for the cleavage site using purely crystallographic data. There are, however, significant limits on conformations of the nucleotides that flank the scissile phosphate. Phosphodiester cleavage requires the 2′-hydroxyl of U(−1) to be positioned for in-line attack at the scissile phosphate. In addition, G1 remains base-paired in helix P1, as supported by extensive structure−function and phylogenetic studies at this position. All naturally occurring HDV-like ribozymes have a purine-pyrimidine base pair at this location (*12*, *13*), and mutagenesis experiments confirm that all combinations of purine-pyrimidine base pairs, including G·U and A^+·C wobble pairs, are tolerated, but pyrimidine-purine or purine-purine base pairs will not support maximal activity (*14*, *15*, *57*−*60*). These data suggest that the base pair between positions 1 and 37 must form and that there must be some requirement for the purine structure at position 1. Finally, U(−1) cannot overlap with the covalent structure of the HDV active site.

To explore the possible locations of the nucleotide at position −1, we compared the crystal structure of the HDV ribozyme at the G1 nucleotide with the conformation of the scissile phosphate, upstream nucleotide, and downstream nucleotide in the hairpin, hammerhead, and glmS ribozymes. The conformation of the cleavage site in the hairpin ribozyme (*41*, *42*, *61*) is not compatible with the active site in the HDV ribozyme. Superposition of the nucleotide downstream of the scissile phosphate with G1 of the HDV ribozyme leads to significant steric clashes between the upstream nucleotide and the HDV ribozyme active site (data not shown). Superposition of the nucleotide downstream of the scissile phosphate from the hammerhead ribozyme (*43*) with G1 of the HDV, however, leads to a model for U(−1) and the scissile phosphate that can be well accommodated within the HDV ribozyme active site (Figure 4). The resulting model is in agreement with previous biochemical data and suggests a catalytic strategy for the HDV ribozyme (see Discussion). A list of distances between key atoms is given in Table 2. Superposition of the HDV ribozyme active site with the substrate region of the glmS ribozyme (*44*, *45*) provides a model that is largely similar to that produced with the hammerhead ribozyme but produces a few steric clashes.

Table 2: Distances within the Crystal Structure

atom 1	atom 2	distance (Å)
Mg^{2+}	U(−1) 2′-OH	2.4[a]
Mg^{2+}	U23 *pro*-S_P O	2.1[a]
Mg^{2+}	G1 *pro*-R_P O	2.2
C75 N3	G1 5′O	3.7

[a]In the crystal structure, these atoms were modeled as a water molecule. The distance reported is that between the water molecule and the Mg^{2+} ion.

Is this model supported by the crystallographic data? We were unsuccessful in attempts to refine the model against the diffraction data. This could be the result of positional disorder, reduced occupancy at this position, or dynamics intrinsic to the HDV ribozyme (see Discussion). Nonetheless, there is density in $F_o - F_c$ difference Fourier maps that is consistent with this model at positions corresponding to the scissile phosphate, the deoxyribose U(−1), and the nucleobase of U(−1) (Figure 2 and Figure S3 of the Supporting Information).

DISCUSSION

The crystal structure of the HDV ribozyme described here differs from those in previous studies in that both the scissile phosphate and C75 are present in the active site. As described, the catalytic mechanism most consistent with this structure suggests that prior to cleavage, C75 is protonated and a catalytic metal ion is bound. In the model described here, the N3 atom of C75 is within 3.7 Å of the 5′-bridging oxygen of G1 (Table 2). This distance and previous Raman spectroscopic analysis of these crystals (*21*) are consistent with protonation of C75. We observe that the positively charged C75 N3 atom and Mg^{2+} functionalities are close in space (5.5 Å). This is consistent with previous studies that show these two cations interact electrostatically and thereby could help drive the reaction by ground-state destabilization (*21*, *47*, *51*). It is therefore unlikely that protonation of C75 and metal binding in the active site can occur without the presence of the negatively charged scissile phosphate. In the model of the substrate-bound ribozyme developed here (Figure 4), the scissile phosphate bridges these two positively charged groups, an interaction that is reminiscent of metal−metal positioning in other ribozymes and protein enzymes (*4*−*7*, *62*, *63*).

Although the inhibitor RNA strand near the scissile phosphate is disordered in the electron density maps, there is evidence that it is present within our crystals with reasonable occupancy. First, the catalytic metal ion is seen bound within the active site. This metal is not observed in the structure of the cleaved ribozyme (*23*), although the binding site appears to be intact. As described above, the affinity for the catalytic metal ion is likely to be very low in the absence of the scissile phosphate. Second, there is electron density near the catalytic metal ion that is in good position to be the scissile phosphate, and it is of sufficient intensity (5σ in the $F_o - F_c$ difference Fourier map) to result from an electron-rich phosphate group. Finally, analysis of crystals indicates that the full-length inhibitor strand is at least 50−90% intact (Figure S2 of the Supporting Information). Thus, the crystal structure here provides the first picture of the HDV ribozyme with the invariant C75 nucleotide and the scissile phosphate in the presence of the Mg^{2+} ion.

The pro-R_P Oxygen of the Scissile Phosphate Is an Inner-Sphere Ligand to the Catalytic Mg^{2+} Ion. In the model generated by superposition of the conformation of the hammerhead ribozyme substrate on the HDV ribozyme core, the *pro*-R_P oxygen of the scissile phosphate appears to interact directly with the catalytic metal ion (Figure 4). This interaction is supported crystallographically by ~5σ electron density at this position in the $F_o - F_c$ difference Fourier map (Figure S3 of the Supporting Information). There are also solution biochemical data that support coordination of the *pro*-R_P oxygen by a metal ion: substitution of this atom with a sulfur has been shown to result in a less active population of ribozyme in which 80% of the ribozyme is nonreactive and 20% reacts with kinetics similar to that of the unmodified or *pro*-S_P-modified substrates (*64*). [It is conceivable that the *pro*-R_P-modified substrate sample was contaminated by *pro*-S_P-modified substrate or unmodified RNA, or that the reactive 20% reacted through an alternate, metal-independent channel (*51*).] Interaction of the catalytic Mg^{2+} ion with the scissile phosphate allows for potential close positioning to the nucleophilic 2′-hydroxyl of U(−1). There is a wealth of evidence from the hammerhead ribozyme that implicates an interaction between an active site metal ion and the *pro*-R_P oxygen of the scissile phosphate (*65*−*71*). Thus, the HDV and hammerhead ribozymes may share similarities in their cleavage mechanisms.

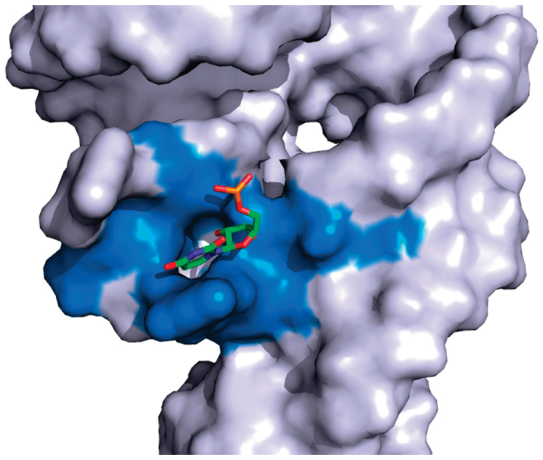

FIGURE 5: HDV ribozyme having an exit site for nucleotides upstream of the scissile phosphate. The crystal structure of the HDV ribozyme is rendered as a molecular surface. U(−1) is drawn as sticks. Nucleotides G1, C22, U23, G25, and G27 (blue) surround U(−1) to create an exit site for the upstream nucleotides. This characteristic likely allows the HDV ribozyme to efficiently fold and function in the context of a long RNA molecule.

A Binding Site for the U(−1) Nucleotide? There does not appear to be a tight binding pocket for the nucleotide upstream of the scissile phosphate. Phylogenetic analysis reveals no sequence specificity for the nucleotide at position −1, suggesting few if any contacts to the nucleobase at position −1 (*14*, *15*, *18*). Indeed, if the upstream product exhibited significant binding, it would be predicted that the HDV ribozyme, like the hammerhead and hairpin ribozymes, would be able to catalyze ligation of the 2′,3′-cyclic phosphate and the 5′-hydroxyl termini. However, HDV-catalyzed ligation reactions cannot be observed (*72*). While the contacts between the ribozyme active site and the nucleotide at position −1 are minimal, there are almost certainly several key contacts that serve to position the 2′-hydroxyl for in-line attack at the scissile phosphate and to enhance the nucleophilicity of the 2′-hydroxyl group. The catalytic metal ion appears to provide one of these contacts, interacting with both the 2′-hydroxyl and *pro*-R_P oxygen of the scissile phosphate, thereby orienting the nucleotide for catalysis.

Binding of the upstream nucleotide U(−1) appears to be further stabilized by base stacking between U(−1) and U23 (Figure 4A). In this study, there is a crystal contact near U23. It was therefore unclear whether the conformation of U23 in the inhibitor-bound form of the HDV ribozyme was native or due to the interaction between neighboring molecules in the crystal. We therefore examined the previously determined crystal structures (Figure S4 of the Supporting Information). In the rhombohedral crystal forms obtained by crystallization of the HDV ribozyme with the U1A protein, there are no crystal contacts near U23. In these structures, we see that U23 is flipped out into solution and adopts a variety of conformations depending on the context. These conformations are not compatible with base stacking of U(−1) and U23. However, examination of the electron density for the cleaved, product-bound HDV ribozyme (PDB entry 1CX0) does reveal electron density compatible with a structure in which U23 is poised to stack on U(−1) (Figure S3 of the Supporting Information). This electron density had previously been interpreted as a Mg^{2+} ion but is more likely to represent an alternate conformation for U23. Thus, it seems likely that

stacking between U23 and U(−1) occurs in solution and is not an artifact of crystal contacts. Consistent with this interaction, HDV ribozyme cleavage of a substrate with an abasic nucleotide at position −1 occurs with a rate constant ~10-fold lower than that of a natural RNA substrate (*73*). Base stacking interactions between the ribozyme active site and the base at position −1 would likely provide a small amount of favorable binding energy for the upstream nucleotide without requiring sequence specificity.

The HDV Ribozyme Has an Exit Site for the Upstream RNA Product. Most small ribozymes, including the hairpin, hammerhead, and VS types, orient their substrate RNA by formation of base pairs both upstream and downstream of the scissile phosphate. In contrast, the HDV ribozyme base pairs to its substrate only downstream of the scissile phosphate. There is no tight binding site for the upstream nucleotides, and consequently, no reverse reaction is observed. Furthermore, the HDV ribozyme has evolved to fold and function within a long RNA transcript. Thus, it seemed likely that there is an exit from the HDV ribozyme active site that would accommodate an RNA long enough to serve as a mRNA. In contrast to the structure of the inactive C75U precleaved RNA, we observe in our model a sharp turn at the scissile phosphate that facilitates egress of the upstream RNA sequence from the active site (Figure 4). Nucleotides involved in forming the exit site are G1, C22, U23, G25, and G27. The exit site (Figure 5) points the phosphate group of the upstream nucleotide out into solution. This strategy would allow the HDV ribozyme to fold more efficiently in the context of a long RNA strand without depending on a guide sequence to form a base pair with the upstream nucleotides. It is notable that with a RNA molecule containing 54 upstream nucleotides, the first 17 nucleotides upstream of the cleavage site are single-stranded, potentially facilitating this egress (*74*).

A Catalytic Role for the Interaction between the Mg^{2+} Ion and the 2′-Hydroxyl of U(−1). The reaction mechanism of the HDV ribozyme has been extensively studied using solution biochemical experiments. Analysis of the pH−rate profile, divalent metal ion preferences, $Co(NH_3)_6^{3+}$ inhibition, the response to modified substrates, and proton inventory experiments have suggested a mechanism in which the 5′-oxyanion leaving group is stabilized by a proton transfer by C75 (summarized in ref *75*). C75 has a pK_a shifted ~2 pH units to ≥6, which gives it the characteristic of a good general acid (*20*, *21*).

Analysis of the pH−rate profile in the presence and absence of Mg^{2+} required a Mg^{2+}-dependent pK_a that was ≥9, the experimental limit of pH−rate profiles because of alkaline denaturation of base pairing. This pK_a is consistent with a Mg^{2+}-bound water, which has an unperturbed pK_a of 11.42 (*76*), serving as a Brønsted base in the cleavage reaction (*20*). In addition, $Co(NH_3)_6^{3+}$, which is a mimic of a hydrated Mg^{2+} ion (*77*−*80*), is a strong inhibitor of the HDV ribozyme, and the mechanism of this inhibition is competitive with Mg^{2+} ion (*17*, *47*). These experiments and others led to a model in which a water molecule bound to a largely hydrated Mg^{2+} ionizes to Mg^{2+}-bound hydroxide and serves as the general base in the cleavage reaction (*20*).

In the model of the precleavage substrate-bound state developed here, however, the 2′-hydroxyl of the upstream nucleotide is best positioned as an inner-sphere ligand to the catalytic Mg^{2+} ion; i.e., it may not interact through a water molecule (Table 2). This model suggests that, under biologically relevant Mg^{2+}-containing conditions, the 2′-hydroxyl nucleophile may be activated by a Lewis acid mechanism. This mechanism is fully consistent with the pH−rate profiles as well. Hydroxide ion, which has a pK_a of 15.7 (i.e., >9), could deprotonate the 2′-hydroxyl in a rapid equilibrium or concerted deprotonation step. Indeed, the involvement of hydroxide ion as a specific base in the HDV ribozyme mechanism has been recently provided by solvent isotope and proton inventory experiments in the absence of divalent ions (*54*) and is also fully consistent with proton inventories of two in the presence of divalent ions (*81*). Moreover, if hydroxide ion acts to deprotonate the 2′-hydroxyl, then the pK_a of the metal ion-bound water would not influence the rate of the reaction.[1] In fact, this is largely what has been observed in prior biochemical studies: the reaction rate is similar (or slightly faster) in Ca^{2+} and Mg^{2+} (2-fold faster without added Na^+ and equal in 1 M Na^+) (*17*) despite the respective pK_a values for metal-bound waters being 12.70 and 11.42 (*76*), and adding 1 M NaCl to the reaction mixture allows Zn^{2+} to react as fast as Mg^{2+} and Ca^{2+} (*17*), despite a pK_a on Zn^{2+}-bound water of just 8.96.[2] In summary, prior pH−rate profile data can be fully explained by a Lewis acid role for the active site divalent ion, with hydroxide ion performing deprotonation—and prior metal rate dependence data are more fully in line with a Lewis acid role than a Brønsted base role for the divalent ion. Nonetheless, we cannot rule out a bridging water without further experiments.

The HDV Ribozyme Uses Two Catalytic Strategies To Achieve Catalysis. Large ribozymes including group I and II introns are metalloenzymes, as established by metal specificity switch experiments and recent crystallographic studies. It was therefore widely believed that all ribozymes would follow suit and be metalloenzymes. However, Scott and co-workers surprisingly showed that the small nucleolytic ribozymes, such as the hammerhead, hairpin, VS, and HDV ribozymes, function in the absence of divalent cations as long as the ionic strength of the buffer is sufficient to stabilize tertiary structure (*9*, *20*, *68*, *82*). As a result, the paradigm was revised to a model in which the nucleolytic ribozymes do not use metal ions to catalyze their cleavage. Indeed, metal ions are not observed in the active sites of the hairpin or glmS ribozymes (*41*, *42*, *44*, *45*). The active site of the hammerhead ribozyme contains a metal ion that contributes structurally to the active site and may contribute to catalysis through a proton chain (*42*) or may be more directly involved in stabilizing the 5′-hydroxyl leaving group in the cleavage reaction (*71*, *83*).

The model for the HDV ribozyme presented here differs significantly from all of the previously studied small ribozyme crystal structures in that a magnesium ion is positioned in the active site in such a way that it can interact directly with the substrate RNA. This observation suggests that this RNA uses strategies common to both large and other small ribozymes. The metal binding site is similar to that observed in group I and group II intron crystal structures in that a single metal ion serves as a ligand to both a nonbridging oxygen atom from the scissile phosphate and the nucleophile (*4*−*7*, *63*, *84*−*86*). Thus, the mechanism for the HDV ribozyme proposed here represents a

[1] von Hippel and co-workers described a scenario in which Lewis acid catalysis demands faster reactivity in Mg^{2+} than Ca^{2+} for another small ribozyme (*87*). However, their model required rate-limiting deprotonation of the 2′-OH, which is not consistent with studies on the HDV ribozyme that reveal proton inventories of two and a dependence of rate on the pK_a of C75; moreover, the HDV ribozyme reacts the same or slower in Mg^{2+} than in Ca^{2+}.

[2] It was previously realized that this effect did not fit expectations for a Brønsted base role for metal-bound waters, but it was suggested that this could be due to the additional and idiosyncratic roles of RNA folding that most divalent ions serve.

hybrid between the metal-mediated catalysis observed for the large ribozymes and the nucleobase-mediated catalysis observed within the hairpin and VS ribozymes.

A Structural Role for the N7 Atom of G1. In naturally occurring versions of the HDV ribozyme, the cleavage site base pair is strictly limited to purine-pyrimidine pairs, although both wobble and Watson−Crick geometries can be accommodated. Comparison of G-C, A-U, G·U, and A^+·C base pairs, all of which are reactive (*60*), reveals only a single consistent feature, the N7 atom of the purine ring. Biochemical experiments reveal that an atomic mutation of the N7 atom to a carbon results in modest reductions in metal binding and activity under restrictive conditions, while accompanying Raman spectroscopy suggests that metal binding and Mg^{2+}−N7 interactions are disrupted by this substitution (*40*).

Examination of the structure reveals why position 1 is limited to a purine. Although the electron density is rather poor in this region, there is a ligand to the N7 atom of G1, likely a water (the N7−water distance is 3.1 Å), but the difference Fourier maps do not strictly rule out a Mg^{2+} ion in this region (not shown). Given that the metal dependence for the reaction is quite loose (*16*, *17*), with most divalents and many transition metals acting similarly with respect to rate, if there were a metal ion in this region it might be quite labile in its kinetics and difficult to observe in the structure. The other ligands to the ordered water near the N7 atom of G1 are the *pro-*R_P oxygen of G76 (2.6 Å) and the 2′-hydroxyl of C75 (3.1 Å) (not shown). Thus, the N7 at position 1 helps stabilize the conformation of the active site through solvent-mediated interactions with C75 and G76. Disrupting this network has a measurable effect on catalytic activity (*58*, *59*). If a pyrimidine were present at position 1, the substitution of a six-membered ring for the five-membered ring and the exocyclic amine (on a C) or the keto oxygen (on a U) would disrupt this network of hydrogen bonds and perturb the active site structure.

Why Does the Inhibitor Exhibit Crystallographic Disorder? The HDV ribozyme has a remarkable lack of specificity in many regards. It has no upstream guide sequence and no sequence specificity for the nucleotide at position −1 (*14*, *15*), will cleave with most divalent ions (*16*, *17*), and readily cleaves a 2′,5′ phosphodiester linkage (*18*). These observations are consistent with lack of a highly ordered cleavage site. As such, dynamics may be inherent to this ribozyme and perhaps even essential to its mechanism. Future studies of MD simulations and additional crystal structures will be necessary to address this potentially important issue.

ACKNOWLEDGMENT

We thank Shu-ichi Nakano, Katsu Murakami, Nancy Horton, Victoria DeRose, and Jeff Bolin for helpful discussions and the beamline staff at SER-CAT, LS-CAT, and GM/CA-CAT for assistance with data collection.

SUPPORTING INFORMATION AVAILABLE

Representative electron density for the inhibitor RNA strand (Figure S1), analysis of RNA integrity in HDV ribozyme crystals (Figure S2), difference Fourier maps near the cleavage site (Figure S3), comparison of the location of U23 in the inhibited and cleaved structures of the HDV ribozyme (Figure S4), and summary of data collection statistics by resolution shell (Table S1). This material is available free of charge via the Internet at http://pubs.acs.org.

REFERENCES

1. Fedor, M. J. (2009) Comparative enzymology and structural biology of RNA self-cleavage. *Annu. Rev. Biophys. 38*, 271–299.
2. Cech, T. R. (2009) Evolution of Biological Catalysis: Ribozyme to RNP Enzyme. *Cold Spring Harbor Symp. Quant. Biol.* (in press).
3. DeRose, V. J. (2003) Metal ion binding to catalytic RNA molecules. *Curr. Opin. Struct. Biol. 13*, 317–324.
4. Adams, P. L., Stahley, M. R., Kosek, A. B., Wang, J., and Strobel, S. A. (2004) Crystal structure of a self-splicing group I intron with both exons. *Nature 430*, 45–50.
5. Guo, F., Gooding, A. R., and Cech, T. R. (2004) Structure of the *Tetrahymena* ribozyme: Base triple sandwich and metal ion at the active site. *Mol. Cell 16*, 351–362.
6. Golden, B. L., Kim, H., and Chase, E. (2005) Crystal structure of a phage Twort group I ribozyme-product complex. *Nat. Struct. Mol. Biol. 12*, 82–89.
7. Stahley, M. R., and Strobel, S. A. (2005) Structural evidence for a two-metal-ion mechanism of group I intron splicing. *Science 309*, 1587–1590.
8. Bevilacqua, P. C., and Yajima, R. (2006) Nucleobase catalysis in ribozyme mechanism. *Curr. Opin. Chem. Biol. 10*, 455–464.
9. Murray, J. B., Seyhan, A. A., Walter, N. G., Burke, J. M., and Scott, W. G. (1998) The hammerhead, hairpin and VS ribozymes are catalytically proficient in monovalent cations alone. *Chem. Biol. 5*, 587–595.
10. Sharmeen, L., Kuo, M. Y., Dinter-Gottlieb, G., and Taylor, J. (1988) Antigenomic RNA of human hepatitis delta virus can undergo self-cleavage. *J. Virol. 62*, 2674–2679.
11. Kuo, M. Y., Sharmeen, L., Dinter-Gottlieb, G., and Taylor, J. (1988) Characterization of self-cleaving RNA sequences on the genome and antigenome of human hepatitis delta virus. *J. Virol. 62*, 4439–4444.
12. Salehi-Ashtiani, K., Luptak, A., Litovchick, A., and Szostak, J. W. (2006) A genomewide search for ribozymes reveals an HDV-like sequence in the human CPEB3 gene. *Science 313*, 1788–1792.
13. Webb, C. H., Riccitelli, N. J., Ruminski, D. J., and Luptak, A. (2009) Widespread occurrence of self-cleaving ribozymes. *Science 326*, 953.
14. Perrotta, A. T., and Been, M. D. (1996) Core sequences and a cleavage site wobble pair required for HDV antigenomic ribozyme self-cleavage. *Nucleic Acids Res. 24*, 1314–1321.
15. Been, M. D., and Wickham, G. S. (1997) Self-cleaving ribozymes of hepatitis delta virus RNA. *Eur. J. Biochem. 247*, 741–753.
16. Suh, Y. A., Kumar, P. K., Taira, K., and Nishikawa, S. (1993) Self-cleavage activity of the genomic HDV ribozyme in the presence of various divalent metal ions. *Nucleic Acids Res. 21*, 3277–3280.
17. Nakano, S., Cerrone, A. L., and Bevilacqua, P. C. (2003) Mechanistic characterization of the HDV genomic ribozyme: Classifying the catalytic and structural metal ion sites within a multichannel reaction mechanism. *Biochemistry 42*, 2982–2994.
18. Shih, I. H., and Been, M. D. (1999) Ribozyme cleavage of a 2,5-phosphodiester linkage: Mechanism and a restricted divalent metal-ion requirement. *RNA 5*, 1140–1148.
19. Perrotta, A. T., Shih, I., and Been, M. D. (1999) Imidazole rescue of a cytosine mutation in a self-cleaving ribozyme. *Science 286*, 123–126.
20. Nakano, S., Chadalavada, D. M., and Bevilacqua, P. C. (2000) General acid-base catalysis in the mechanism of a hepatitis delta virus ribozyme. *Science 287*, 1493–1497.
21. Gong, B., Chen, J. H., Chase, E., Chadalavada, D. M., Yajima, R., Golden, B. L., Bevilacqua, P. C., and Carey, P. R. (2007) Direct measurement of a pK_a near neutrality for the catalytic cytosine in the genomic HDV ribozyme using Raman crystallography. *J. Am. Chem. Soc. 129*, 13335–13342.
22. Perrotta, A. T., Wadkins, T. S., and Been, M. D. (2006) Chemical rescue, multiple ionizable groups, and general acid-base catalysis in the HDV genomic ribozyme. *RNA 12*, 1282–1291.
23. Ferre-D'Amare, A. R., Zhou, K., and Doudna, J. A. (1998) Crystal structure of a hepatitis delta virus ribozyme. *Nature 395*, 567–574.
24. Wadkins, T. S., Perrotta, A. T., Ferre-D'Amare, A. R., Doudna, J. A., and Been, M. D. (1999) A nested double pseudoknot is required for self-cleavage activity of both the genomic and antigenomic hepatitis delta virus ribozymes. *RNA 5*, 720–727.
25. Perrotta, A. T., and Been, M. D. (1991) A pseudoknot-like structure required for efficient self-cleavage of hepatitis delta virus RNA. *Nature 350*, 434–436.
26. Das, S. R., and Piccirilli, J. A. (2005) General acid catalysis by the hepatitis delta virus ribozyme. *Nat. Chem. Biol. 1*, 45–52.

27. Ke, A., Zhou, K., Ding, F., Cate, J. H., and Doudna, J. A. (2004) A conformational switch controls hepatitis delta virus ribozyme catalysis. *Nature 429*, 201–205.
28. Banas, P., Rulisek, L., Hanosova, V., Svozil, D., Walter, N. G., Sponer, J., and Otyepka, M. (2008) General base catalysis for cleavage by the active-site cytosine of the hepatitis delta virus ribozyme: QM/MM calculations establish chemical feasibility. *J. Phys. Chem. 112*, 11177–11187.
29. Krasovska, M. V., Sefcikova, J., Spackova, N., Sponer, J., and Walter, N. G. (2005) Structural dynamics of precursor and product of the RNA enzyme from the hepatitis delta virus as revealed by molecular dynamics simulations. *J. Mol. Biol. 351*, 731–748.
30. Golden, B. L., Podell, E. R., Gooding, A. R., and Cech, T. R. (1997) Crystals by design: A strategy for crystallization of a ribozyme derived from the *Tetrahymena* group I intron. *J. Mol. Biol. 270*, 711–723.
31. Otwinowski, Z., and Minor, W. (1997) Processing of X-ray Diffraction Data Collected in Oscillation Mode. In Methods in Enzymology, Macromolecular Crystallography, Part A (Carter, C. W. J., and Sweet, R. M., Eds.) pp 307−326, Academic Press, New York.
32. Collaborative Computational Project, Number 4 (1994) The CCP4 Suite: Programs for Protein Crystallography. *Acta Crystallogr. D50*, 760–763.
33. Brunger, A. T. (2007) Version 1.2 of the Crystallography and NMR system. *Nat. Protoc. 2*, 2728–2733.
34. Brunger, A. T., Adams, P. D., Clore, G. M., DeLano, W. L., Gros, P., Grosse-Kunstleve, R. W., Jiang, J. S., Kuszewski, J., Nilges, M., Pannu, N. S., Read, R. J., Rice, L. M., Simonson, T., and Warren, G. L. (1998) Crystallography & NMR system: A new software suite for macromolecular structure determination. *Acta Crystallogr. D54*, 905–921.
35. Adams, P. D., Afonine, P. V., Bunkoczi, G., Chen, V. B., Davis, I. W., Echols, N., Headd, J. J., Hung, L. W., Kapral, G. J., Grosse-Kunstleve, R. W., McCoy, A. J., Moriarty, N. W., Oeffner, R., Read, R. J., Richardson, D. C., Richardson, J. S., Terwilliger, T. C., and Zwart, P. H. (2010) PHENIX: A comprehensive Python-based system for macromolecular structure solution. *Acta Crystallogr. D66*, 213–221.
36. DeLano, W. L. (2007) The Pymol Molecular Graphics System, DeLano Scientific, San Carlos, CA.
37. Jones, T. A., Zou, J. Y., Cowan, S. W., and Kjeldgaard, M. (1991) Improved methods for building protein models in electron density maps and the location of errors in these models. *Acta Crystallogr. 47* (Part 2), 110–119.
38. Smith, J. B., and Dinter-Gottlieb, G. (1991) Antigenomic hepatitis delta virus ribozymes self-cleave in 18 M formamide. *Nucleic Acids Res. 19*, 1285–1289.
39. Brown, T. S., Chadalavada, D. M., and Bevilacqua, P. C. (2004) Design of a highly reactive HDV ribozyme sequence uncovers facilitation of RNA folding by alternative pairings and physiological ionic strength. *J. Mol. Biol. 341*, 695–712.
40. Chen, J. H., Gong, B., Bevilacqua, P. C., Carey, P. R., and Golden, B. L. (2009) A catalytic metal ion interacts with the cleavage site G·U wobble in the HDV ribozyme. *Biochemistry 48*, 1498–1507.
41. Rupert, P. B., and Ferre-D'Amare, A. R. (2001) Crystal structure of a hairpin ribozyme-inhibitor complex with implications for catalysis. *Nature 410*, 780–786.
42. Alam, S., Grum-Tokars, V., Krucinska, J., Kundracik, M. L., and Wedekind, J. E. (2005) Conformational heterogeneity at position U37 of an all-RNA hairpin ribozyme with implications for metal binding and the catalytic structure of the S-turn. *Biochemistry 44*, 14396–14408.
43. Martick, M., and Scott, W. G. (2006) Tertiary contacts distant from the active site prime a ribozyme for catalysis. *Cell 126*, 309–320.
44. Klein, D. J., and Ferre-D'Amare, A. R. (2006) Structural basis of glmS ribozyme activation by glucosamine-6-phosphate. *Science 313*, 1752–1756.
45. Cochrane, J. C., Lipchock, S. V., and Strobel, S. A. (2007) Structural investigation of the GlmS ribozyme bound to its catalytic cofactor. *Chem. Biol. 14*, 97–105.
46. Gong, B., Chen, Y., Christian, E. L., Chen, J. H., Chase, E., Chadalavada, D. M., Yajima, R., Golden, B. L., Bevilacqua, P. C., and Carey, P. R. (2008) Detection of innersphere interactions between magnesium hydrate and the phosphate backbone of the HDV ribozyme using Raman crystallography. *J. Am. Chem. Soc. 130*, 9670–9672.
47. Gong, B., Chen, J. H., Bevilacqua, P. C., Golden, B. L., and Carey, P. R. (2009) Competition between $Co(NH_3)_6^{3+}$ and inner sphere Mg^{2+} ions in the HDV ribozyme. *Biochemistry 48*, 11961–11970.
48. Burkard, M. E., Turner, D. H., and Tinoco, I. (1999) Structures of Base Pairs Involving at Least Two Hydrogen Bonds. In RNA World (Gesteland, R. F., Cech, T. R., and Atkins, J. F., Eds.) 2nd ed., pp 675−680, Cold Spring Harbor Laboratory Press, Plainview, NY.
49. Leontis, N. B., and Westhof, E. (2001) Geometric nomenclature and classification of RNA base pairs. *RNA 7*, 499–512.
50. Ferre-D'Amare, A. R., and Doudna, J. A. (2000) Crystallization and structure determination of a hepatitis delta virus ribozyme: Use of the RNA-binding protein U1A as a crystallization module. *J. Mol. Biol. 295*, 541–556.
51. Nakano, S., Proctor, D. J., and Bevilacqua, P. C. (2001) Mechanistic characterization of the HDV genomic ribozyme: Assessing the catalytic and structural contributions of divalent metal ions within a multichannel reaction mechanism. *Biochemistry 40*, 12022–12038.
52. Perrotta, A. T., and Been, M. D. (2007) A single nucleotide linked to a switch in metal ion reactivity preference in the HDV ribozymes. *Biochemistry 46*, 5124–5130.
53. Nakano, S., and Bevilacqua, P. C. (2007) Mechanistic characterization of the HDV genomic ribozyme: A mutant of the C41 motif provides insight into the positioning and thermodynamic linkage of metal ions and protons. *Biochemistry 46*, 3001–3012.
54. Cerrone-Szakal, A. L., Siegfried, N. A., and Bevilacqua, P. C. (2008) Mechanistic characterization of the HDV genomic ribozyme: Solvent isotope effects and proton inventories in the absence of divalent metal ions support C75 as the general acid. *J. Am. Chem. Soc. 130*, 14504–14520.
55. Tanner, N. K., Schaff, S., Thill, G., Petit-Koskas, E., Crain-Denoyelle, A. M., and Westhof, E. (1994) A three-dimensional model of hepatitis delta virus ribozyme based on biochemical and mutational analyses. *Curr. Biol. 4*, 488–498.
56. Chin, K., Sharp, K. A., Honig, B., and Pyle, A. M. (1999) Calculating the electrostatic properties of RNA provides new insights into molecular interactions and function. *Nat. Struct. Biol. 6*, 1055–1061.
57. Wu, H. N., and Huang, Z. S. (1992) Mutagenesis analysis of the self-cleavage domain of hepatitis delta virus antigenomic RNA. *Nucleic Acids Res. 20*, 5937–5941.
58. Wu, H. N., Lee, J. Y., Huang, H. W., Huang, Y. S., and Hsueh, T. G. (1993) Mutagenesis analysis of a hepatitis delta virus genomic ribozyme. *Nucleic Acids Res. 21*, 4193–4199.
59. Nishikawa, F., Fauzi, H., and Nishikawa, S. (1997) Detailed analysis of base preferences at the cleavage site of a trans-acting HDV ribozyme: A mutation that changes cleavage site specificity. *Nucleic Acids Res. 25*, 1605–1610.
60. Cerrone-Szakal, A. L., Chadalavada, D. M., Golden, B. L., and Bevilacqua, P. C. (2008) Mechanistic characterization of the HDV genomic ribozyme: The cleavage site base pair plays a structural role in facilitating catalysis. *RNA 14*, 1746–1760.
61. Salter, J., Krucinska, J., Alam, S., Grum-Tokars, V., and Wedekind, J. E. (2006) Water in the active site of an all-RNA hairpin ribozyme and effects of Gua8 base variants on the geometry of phosphoryl transfer. *Biochemistry 45*, 686–700.
62. Steitz, T. A., and Steitz, J. A. (1993) A general two-metal-ion mechanism for catalytic RNA. *Proc. Natl. Acad. Sci. U.S.A. 90*, 6498–6502.
63. Shan, S., Kravchuk, A. V., Piccirilli, J. A., and Herschlag, D. (2001) Defining the catalytic metal ion interactions in the *Tetrahymena* ribozyme reaction. *Biochemistry 40*, 5161–5171.
64. Fauzi, H., Kawakami, J., Nishikawa, F., and Nishikawa, S. (1997) Analysis of the cleavage reaction of a trans-acting human hepatitis delta virus ribozyme. *Nucleic Acids Res. 25*, 3124–3130.
65. Dahm, S. C., and Uhlenbeck, O. C. (1991) Role of divalent metal ions in the hammerhead RNA cleavage reaction. *Biochemistry 30*, 9464–9469.
66. Slim, G., and Gait, M. J. (1991) Configurationally defined phosphorothioate-containing oligoribonucleotides in the study of the mechanism of cleavage of hammerhead ribozymes. *Nucleic Acids Res. 19*, 1183–1188.
67. Wang, S., Karbstein, K., Peracchi, A., Beigelman, L., and Herschlag, D. (1999) Identification of the hammerhead ribozyme metal ion binding site responsible for rescue of the deleterious effect of a cleavage site phosphorothioate. *Biochemistry 38*, 14363–14378.
68. O'Rear, J. L., Wang, S., Feig, A. L., Beigelman, L., Uhlenbeck, O. C., and Herschlag, D. (2001) Comparison of the hammerhead cleavage reactions stimulated by monovalent and divalent cations. *RNA 7*, 537–545.
69. Osborne, E. M., Schaak, J. E., and Derose, V. J. (2005) Characterization of a native hammerhead ribozyme derived from schistosomes. *RNA 11*, 187–196.
70. Boots, J. L., Canny, M. D., Azimi, E., and Pardi, A. (2008) Metal ion specificities for folding and cleavage activity in the Schistosoma hammerhead ribozyme. *RNA 14*, 2212–2222.

71. Osborne, E. M., Ward, W. L., Ruehle, M. Z., and DeRose, V. J. (2009) The identity of the nucleophile substitution may influence metal interactions with the cleavage site of the minimal hammerhead ribozyme. *Biochemistry 48*, 10654–10664.
72. Wadkins, T. S., and Been, M. D. (2002) Ribozyme activity in the genomic and antigenomic RNA strands of hepatitis delta virus. *Cell. Mol. Life Sci. 59*, 112–125.
73. Shih, I., and Been, M. D. (2001) Energetic contribution of non-essential 5′ sequence to catalysis in a hepatitis delta virus ribozyme. *EMBO J. 20*, 4884–4891.
74. Chadalavada, D. M., Knudsen, S. M., Nakano, S., and Bevilacqua, P. C. (2000) A role for upstream RNA structure in facilitating the catalytic fold of the genomic hepatitis delta virus ribozyme. *J. Mol. Biol. 301*, 349–367.
75. Strobel, S. A. (2005) Ribonucleic general acid. *Nat. Chem. Biol. 1*, 5–6.
76. Feig, A. L., and Uhlenbeck, O. C. (1999) The role of metal ions in RNA biochemistry. In The RNA World (Gesteland, R. F., Cech, T. R., and Atkins, J. F., Eds.) 2nd ed., pp 287−319, Cold Spring Harbor Laboratory Press, Plainview, NY.
77. Basolo, R., and Pearson, R. G. (1988) Mechanisms of Inorganic Reactions, John Wiley & Sons, New York.
78. Hampel, A., and Cowan, J. A. (1997) A unique mechanism for RNA catalysis: The role of metal cofactors in hairpin ribozyme cleavage. *Chem. Biol. 4*, 513–517.
79. Nesbitt, S., Hegg, L. A., and Fedor, M. J. (1997) An unusual pH-independent and metal-ion-independent mechanism for hairpin ribozyme catalysis. *Chem. Biol. 4*, 619–630.
80. Young, K. J., Gill, F., and Grasby, J. A. (1997) Metal ions play a passive role in the hairpin ribozyme catalysed reaction. *Nucleic Acids Res. 25*, 3760–3766.
81. Nakano, S., and Bevilacqua, P. C. (2001) Proton inventory of the genomic HDV ribozyme in Mg^{2+}-containing solutions. *J. Am. Chem. Soc. 123*, 11333–11334.
82. Curtis, E. A., and Bartel, D. P. (2001) The hammerhead cleavage reaction in monovalent cations. *RNA 7*, 546–552.
83. Lee, T. S., Silva Lopez, C., Giambasu, G. M., Martick, M., Scott, W. G., and York, D. M. (2008) Role of Mg^{2+} in hammerhead ribozyme catalysis from molecular simulation. *J. Am. Chem. Soc. 130*, 3053–3064.
84. Gordon, P. M., Sontheimer, E. J., and Piccirilli, J. A. (2000) Kinetic characterization of the second step of group II intron splicing: role of metal ions and the cleavage site 2′-OH in catalysis. *Biochemistry 39*, 12939–12952.
85. Gordon, P. M., Fong, R., and Piccirilli, J. A. (2007) A second divalent metal ion in the group II intron reaction center. *Chem. Biol. 14*, 607–612.
86. Toor, N., Keating, K. S., Taylor, S. D., and Pyle, A. M. (2008) Crystal structure of a self-spliced group II intron. *Science 320*, 77–82.
87. Pontius, B. W., Lott, W. B., and von Hippel, P. H. (1997) Observations on catalysis by hammerhead ribozymes are consistent with a two-divalent-metal-ion mechanism. *Proc. Natl. Acad. Sci. U.S.A. 94*, 2290–2294.